Journal of Alloys and Compounds 698 (2017) 1077–1085

Contents lists available at ScienceDirect

Journal of Alloys and Compounds

journal homepage: http://www.elsevier.com/locate/jalcom

Synthesis, characterization and catalytic sorption activity of various method prepared magnetite (Fe_3O_4) nanoparticle deposition on porous BiMnOx nanotubes

Jothi Ramalingam Rajabathar [a, *], Judith J. Vijaya [b], Arunachalam Prabakaran [c], Zuheir A. Issa [a], Ayman M. Atta [a], A.O. Ezzat [a], Abdullah M. Al-Mayouf [c], Hamad A. Al-Lohedan [a]

[a] Chemistry Department, College of Science, King Saud University, P.O. Box 2455, Riyadh 11451, Saudi Arabia
[b] Electrochemistry Research Group, Chemistry Department, King Saud University, Riyadh 11451, Saudi Arabia
[c] Catalysis & Nanomaterials Research Laboratory, Department of Chemistry, Loyola College (Autonomous), Chennai 600 034, India

ARTICLE INFO

Article history:
Received 12 November 2016
Received in revised form
14 December 2016
Accepted 15 December 2016
Available online 18 December 2016

Keywords:
Bi-MnOx nanotube
Fe_3O_4
Nanoparticles
Electron microscopy
Phenol
Trixton-100

ABSTRACT

Magnetite nanoparticle deposited porous Bi-doped MnOx nanocomposite were prepared by two step co-precipitation and deposition process. Surfactant assisted co-precipitation method is adopted to prepare porous Bi-MnOx nanotube followed by Fe_3O_4 nanoparticle incorporation by ultrasonic assisted deposition method. The role of iodine and EDTA for stabilize the magnetite nanoparticle have been studied. The various method prepared Fe_3O_4 deposited nanocomposite was characterized by X-ray diffraction (XRD), scanning and transmission electron microscopy (SEM & TEM), Fourier transform infrared (FT-IR) spectra and Diffuse reflectance spectroscopy (DRS). XRD patterns are confirm the mixed manganese oxide and bismuth oxide phase formation. XRD and TEM study of individual magnetite nanoparticle prepared at various conditions have also been exploited. Magnetite nanoparticles are incorporated inside the tube structure of BiMnOx and also it acted as template for formation of magnetite nanorods. The nanotube morphology clearly observed using HR-TEM images. The band gap values of all prepared samples were characterized by DRS absorbance spectra. The reduce band gap values (1.97 eV–2.3 eV) are obtained for certain magnetite deposited BiMnOx nanocomposite. The as prepared sample are further tested for phenol sorption capacity and its showing enhanced adsorption capacity.

1. Introduction

Manganese and iron oxides are available in plenty and eco-friendly substance for scientific applications [1,2]. Different type of doped and undoped micro porous MnO_2 and Fe_2O_3 are used successfully for catalytic oxidation reactions and remediation of heavy metal ion contamination [3,4]. In recent years, many synthetic strategies are developed for Iron and MnOx based substance at nanoscale level for potential application in waste water treatment and energy storage super capacitor device development. MnOx nanoparticle is act as efficient electrode materials for ORR in Fuel cell applications [4–6]. Among the transition metal oxides explored, MnO_2 has been extensively investigated due to its abundance, existence in different crystallographic forms (α, β, γ and δ), low cost, ecofriendly nature and high theoretical Cs (1370 F g^{-1}) for the said purpose [7,8]. In spite of being a very good pseudo capacitive material, commercial application of manganese oxide (MnO_2) is limited due to its low electrical conductivity, structural instability and low rate capability [9,10]. Therefore, a composite of MnO_2 with highly conducting material is preferred to overcome these disadvantages of pure MnO_2. In this regard, a composite with MWCNT is preferred owing to its large surface area, good conductivity and entangled mesoporous structure. These unique structural properties of MWCNT would act as conducting backbone for MnO_2 thereby enhancing not only its supercapacitance and stability during cycling but also allowing easy diffusion of the electrolyte ions through the material.

Different variety or types of Iron-containing solids, like nanoparticle of iron [11,12], Iron oxy hydroxide [13], Fe_3O_4 [14] and Fe_2O_3 [15,16] have been used as catalytic materials to degradation

* Corresponding author.
E-mail addresses: rjothiram@gmail.com, jrajabathar@ksu.edu.sa (J.R. Rajabathar).

http://dx.doi.org/10.1016/j.jallcom.2016.12.192
0925-8388/

of environmental pollutant. However, the bulk solids exhibited weak catalytic activity [17] and higher iron leaching [18]. Many strategies have been developed to enhance the activity of heterogeneous Fenton catalyst, such as reducing the size of the catalyst to the nanoscale [17], loading the catalysts on carriers with a high surface area [15,19]. Wei et al. (2015) recently reported facile synthesis of magnetic deposited octahedral molecular sieve (OMS-2) catalyst for removal of organic dyes in aqueous medium using peroxy mono sulfate [20]. Magnetite nanoparticle homogeneously deposited on the surface of OMS-2 and forms the similar morphological shapes after formation of nanocomposite. The prepared magnetite/OMS-2 showing improved surface area and good catalytic degradation activity for various acid-base organic dyes. Magnetic properties of ferrite materials are another interesting aspect for biomedical applications [20]. Vinas et al. (2016) reported Fe_3O_4-coated ferrite core shell NPs for magnetic hyperthermia applications and they compared their records with their single-phase counterparts. In our previous research report related with Functionalized magnetite nanocomposite with polymerizable surfactants are prepared based on cross-linked acrylamide-co-acrylic acid sodium salt copolymer for easy dispersion of magnetite nanoparticles in aqueous medium. The as prepared magnetite/cross linked polymer composites are showing excellent corrosion resistance in acid medium [21]. Ultrasound assisted route synthesis of magnetite nanoparticle provides the hierarchical porous and densely packed composite structures. The porosity not only improves the surface area and also increase fast ion transport and maintain the synergistic effect for achieve superior electrochemical performance. Recently, homogenously dispersed magnetite nanoparticle doped with porous MnO_2 by ultrasound assisted method for supercapcitor applications [22].

Modified magnetite nanoparticles capped with rosin amid oxime are reported previously by our research group and it showing good sorption capacity for removal thorium like radio nuclide [23]. Rosin is used as a bioactive material to modify to prepare diacrylamidoxime triethylene tetralevopimaramide that used to coat on the surface of Fe_3O_4 nanoparticles [24]. The less toxicity and super paramagnetic property of the coated Fe_3O_4 is easily separable from the solution using external magnetic field. To the best of our knowledge magnetite nanoparticle deposited bismuth doped manganese oxides with porous nanotube structure are not reported. The magnetite nanoparticle has coated on nanotubes structure of BiMnOx to enhance its catalytic and electrochemical property. The band gap energy alteration and phenol sorption removal capacity have been studied on magnetite nanoparticle-$BiMnO_x$ nanocomposite.

2. Experimental

2.1. Materials and method

Anhydrous ferric chloride ($FeCl_3$), potassium iodide (KI), EDTA (*N*,*N*′-ethylene diamine diacetic acid tetra hydrate) and ammonium hydroxide (25%) were obtained from sigma aldrich Chemical Company. Trixton-100 is used as non-ionic surfactant to prepare BiMnOx nanotubes. The first step is to prepare pristine BiMnOx by precipitation method using manganese sulfate (19.0 g) bismuth nitrate (24.2 g) are mixed in 75 mL of water and stirred continuously(A). In another beaker 5 mL of Trixton-100 added in 250 mL of water stirred (B). Solution (A) and solution (B) mixed together after some time. The oxidizing agent sodium persulphate (22.8 g dissolved in 25 mL) is added dropwise to the mixed solution followed by dropwise addition of 40 mL of aqueous NH_3 added to form the brown precipitate. Then continue to stir for 12 h and filtered and dry the brown colored precipitate at 120 °C in order to remove the volatile impurities. The resultant solid was calcined at 400 °C for 3 h to form the nanotubes of BiMnOx.

2.2. Variety of magnetite nanoparticle preparation with capping agent

2.2.1. Magnetite nanoparticle preparation in presence and absence

Aqueous solution $FeCl_3$ (40 g, 0.24 mol in distilled water 300 mL) and KI (13.2 g, 0.08 mol dissolved in distilled water 50 mL) were mixed together at room temperature for 1 h under N_2. The solutions were hydrolyzed in the presence and absence of precipitated iodine using 200 mL of 25% ammonia solution at room temperature. The reaction time was extended for 4 h to obtain black and brown colloidal iron oxide solutions which left to settle, filtered, washed with distilled water and ethanol. The percentage yield of the reaction as brownish black precipitate was 95.5%. The magnetite prepared in presence and absence of iodine is designated as 211 and 212, respectively.

2.2.2. Preparation of magnetite capped with excess EDTA

The capping of magnetite with EDTA in the presence of iodine [designated as sample code 213 and 214] was as follows: The iron cations produced from reaction of anhydrous $FeCl_3$ (40 g dissolved in distilled water 300 mL) and KI (13.2 g, dissolved in distilled water 50 mL at room temperature for 1 h.

Tetra sodium EDTA (8 g dissolved in 100 mL of 25% ammonia solution and added to reaction mixture at the same time with 200 mL of ammonia solution after warm the reaction mixture at 45 °C. The reaction mixture was stirred and bubbled with pure N_2 for 4 h until complete black colloidal solutions was formed to isolate the capped magnetite nanoparticle with ultracentrifuge at 12000 rpm without heating. The final product was washed with ethanol and air dried to give a reaction yield percentage of 99.5%. The mole ratio of Fe_3O_4: EDTA is maintained at 4:1 (sample code designated as 213). Another set of sample, the mole ratio of Fe_3O_4: EDTA is maintained at 4:2 was also synthesized for comparative study and the respective sample code designated as 214.

Sample code	Preparation condition
211	Fe_3O_4 nanoparticle prepared in presence of Iodine
212	Fe_3O_4 nanoparticle prepared in presence of Iodine
213	Fe_3O_4 nanoparticle prepared in presence of Iodine + EDTA
214	Fe_3O_4 nanoparticle prepared in presence of Iodine + excess EDTA

2.2.3. Ultrasonic deposition of BiMnOx-magnetite nanocomposite preparation

The appropriate amount (0.1 g) of magnetite nanoparticle (sample code 211 to 214) is mixed with ethanol solution and ultrasonicated for 5 min by applying 20% amplitude of power. After 5–10 min, 1.0 g of as prepared Bi-MnO_x nanotube powder added into the ethanol solution dispersed magnetite. Then the mixed solution ultrasonicate further 10 min, followed by dried at 80 °C.

The XRD pattern of the powder sample are recorded using Miniflex 600. The chemical structure and composition of iron oxide nanoparticles capped with EDTA were confirmed using FTIR (Nicolet spectrophotometer). The morphology and particle size distribution of the nanoparticles were evaluated using Transmission electron microscopy (TEM; JEOL JEM-2100F) and dynamic light scattering (DLS; Brookhaven Instruments system). Branson digital sonifier®400 is used for ultra-sonication process. Diffuse

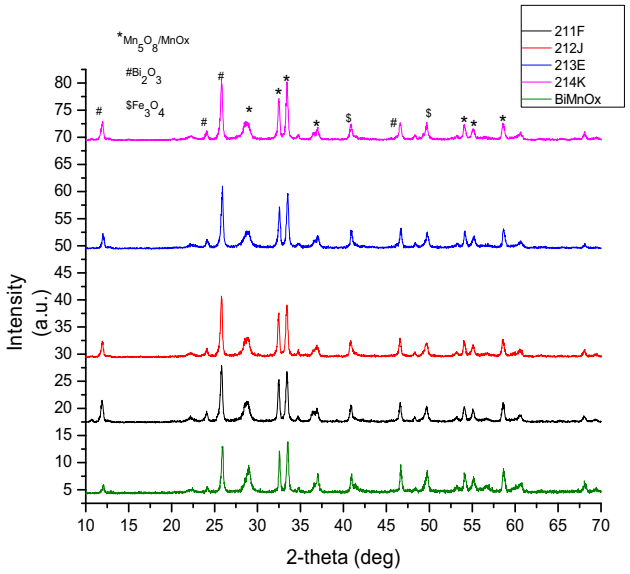

Fig. 1. XRD patteren of Fe_3O_4-BiMnOx nanotube and bulk BiMnOx (green color line). (For interpretation of the references to colour in this figure legend, the reader is referred to the web version of this article.)

reflectance spectroscopy (JASCO UV–Visible spectrophotometer V550 ISV469). Surface area measurement and N_2-sorption isotherms were analyzed by NOVA 2200e model.

3. Results and discussion

The X-ray diffraction pattern of different reaction condition prepared magnetite nanoparticle deposited on Bi-MnOx nanotube are shown in Fig. 1. The mixed metal oxide phase exists in the final nanocomposite catalyst. The crystalline phase marked with different symbol. The pristine Bi-MnOx nanotube XRD phase exist similar to Mn_5O_8 (ICDD 00-039-1218) and similar XRD pattern obtained for magnetite deposited BiMnOx samples [24]. Some reflections are marked (# and $) due to presence of Bi_2O_3 and Fe_3O_4 phase formation. The Ft-IR spectra of magnetite deposited BiMnOx nanocomposite are shown in Fig. 2. The typical peak was found that the appearance of broad band at 570 cm^{-1} due to Fe-O stretching and Mn-O stretching absorption band appear below 500–450 cm^{-1}. The few peaks at 1550–1600 cm^{-1} are due to presence of polymeric carbon in the nanocomposite material.

UV–Vis DRS spectra of all the prepared nanocomposite are shown in Fig. 3 and it's all following similar trend expect sample 214 and 212. The band at 465 nm is slightly more intense compared to other route prepared magnetite. The reduced band gap values are observed for all the prepared nanocomposite. The band gap values are calculated using kubelka munk equation. The preparation route is strongly influence the tuning of band gap value of the nanocomposite materials.

Fig. 4 shows the band gap values of the respective samples, tuning of band gap values are observed due to magnetite nanoparticle deposition on BiMnOx nanotube. The nature of magnetite particle altered by presence of iodine and capping agent after ultrasonic assisted deposition process. Fig. 4a–b shows the increased band gap values for magnetite nanoparticle prepared in presence of iodine and in the absence. EDTA capped magnetite nanoparticle showing reduced band gap values after deposition on BiMnOx nanotube.

It was previously reported that [25–27] that the iron oxides based on Fe_3O_4 (magnetite), γ-Fe_2O_3 (maghemite, ferrimagnetic), was prepared from reaction of KI and $FeCl_3$ in the presence of iodine as confirmed by the following chemical equations:

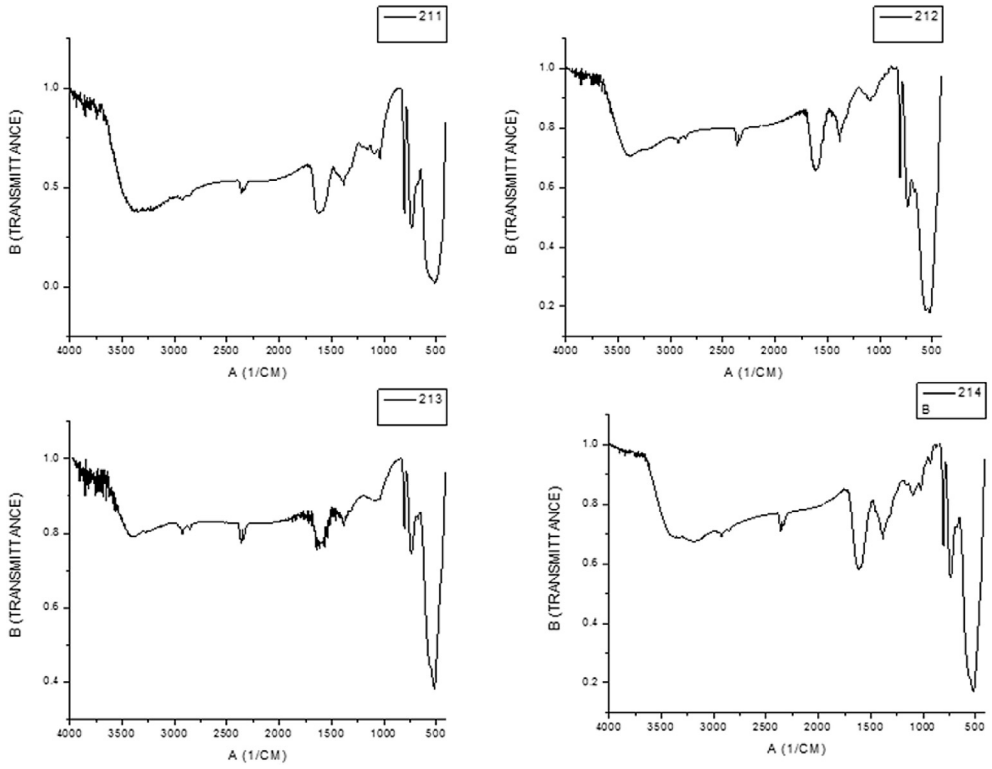

Fig. 2. FT-IR spectra of magnetite deposited BiMnOx nanocomposite.

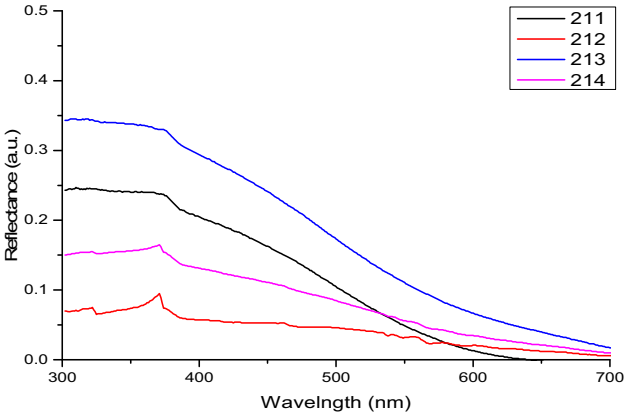

Fig. 3. UV–Vis-DRS spectra of magnetite deposited BiMnOx nanocomposite.

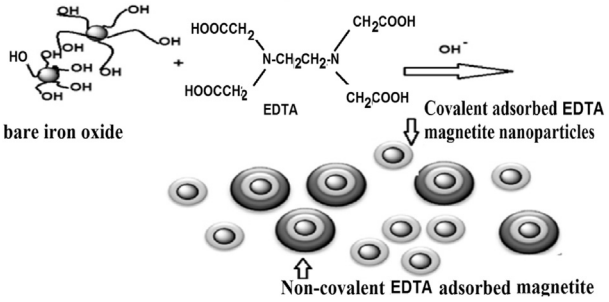

Scheme 1. Preparation of magnetite capped with EDTA.

$$3Fe^{3+} + I^- \rightarrow 2Fe^{3+} + Fe^{2+} + 1/2I_2 \quad (1)$$

$$2Fe^{3+} + Fe^{2+} + 8OH^- \rightarrow Fe_3O_4 + 4H_2O \quad (2)$$

The magnetite (Fe_3O_4) is not very stable and is sensitive to oxidation and is transformed into maghemite (γFe_2O_3) in the presence of oxygen. It was previously reported that when iodine is added to water, the following reaction takes place [28]:

$$I_2\,(1) + H_2O\,(1) \rightarrow OI^-\,(aq) + 2H^+\,(aq) + I^-\,(aq)\,(K = 2.0 \times 10^{-13}) \quad (3)$$

$$I_2 + 2OH^- \rightarrow I^- + IO^- + H_2O\,(K = 30) \quad (4)$$

$$3OI^- \rightarrow 2I^- + IO_3^-\,(K = 1020) \quad (5)$$

It was suggested that IO_3^- is physically adsorbed on iron oxide surfaces to produce more hydroxyl groups which are able to form chemical and physical bonds with different capping agents. It was expected that the chelation of the carboxylate and amine groups of EDTA on the iron oxide surface can either prevent nucleation and thus lead to larger particles or inhibit the growth of the crystal nuclei, leading to small nanoparticles. EDTA contains different

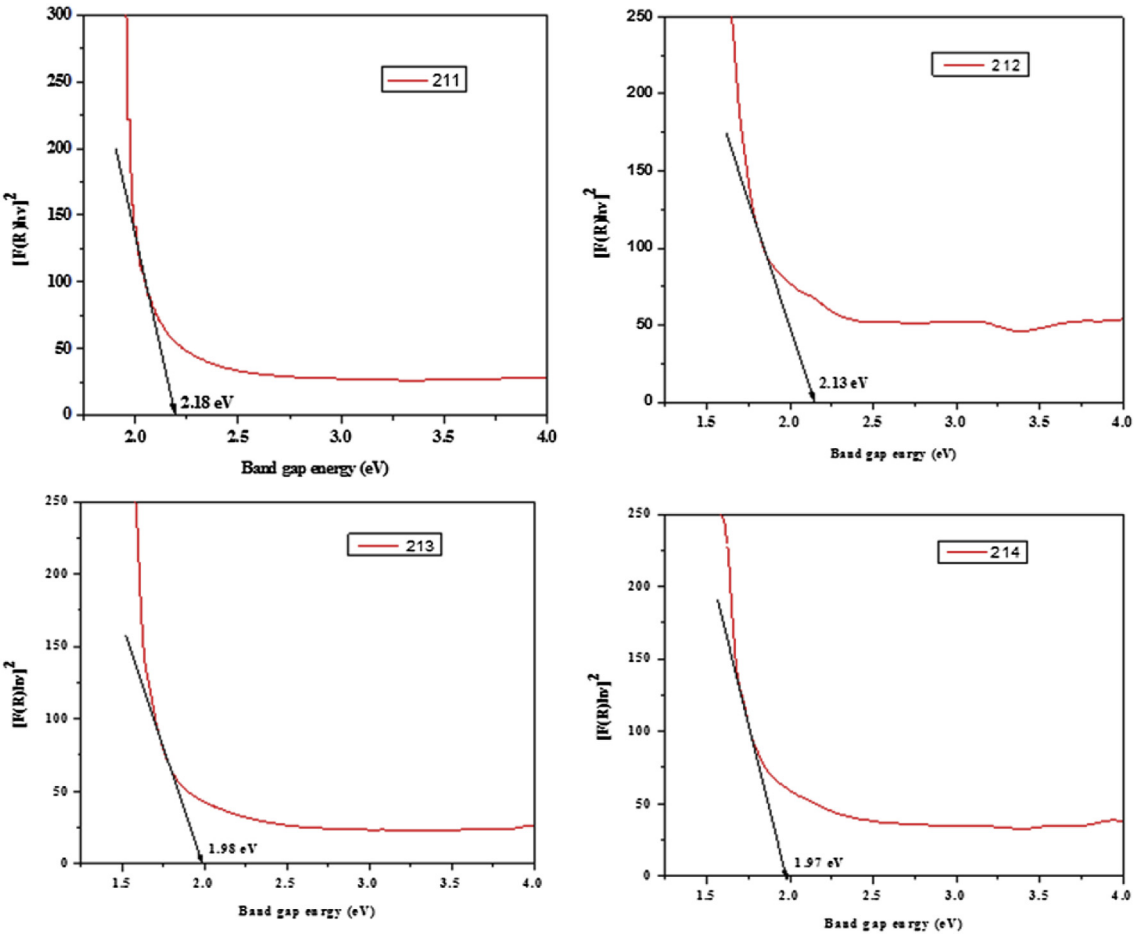

Fig. 4. Band gap diagram of magnetite deposited BiMnOx nanocomposite.

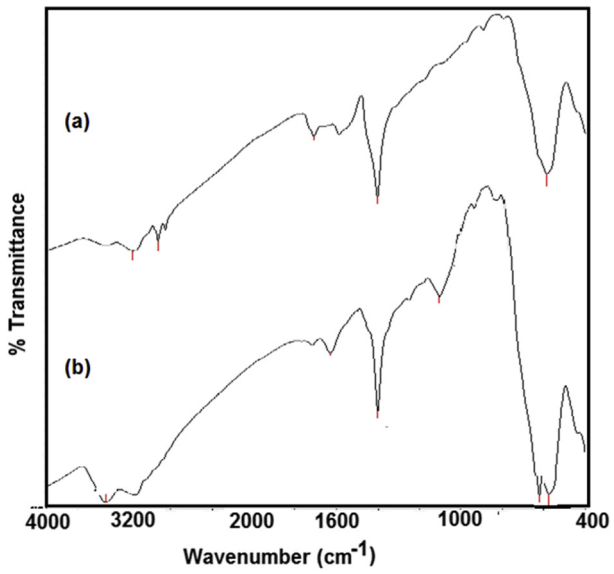

Fig. 5. FTIR spectra of the prepared magnetite (a) presence of EDTA/I_2 and (b) presence of EDTA without I_2.

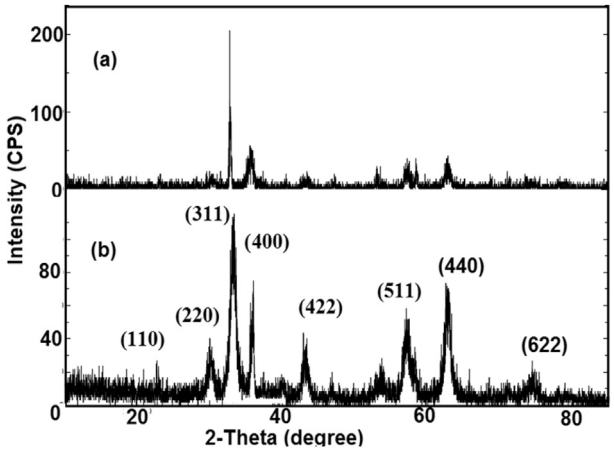

Fig. 6. XRD diffractograms of the prepared magnetite (**a**) presence of EDTA/I_2 and (**b**) presence of EDTA without I_2.

functional groups can be used as a stabilizing agent for magnetite nanoparticles to avoid their agglomeration in the present work. The capping of iron oxides with EDTA can be illustrated by Scheme 1.

The adsorption of EDTA on magnetite nanoparticles (MNPs) was illustrated by several mechanism involving intermolecular hydrogen bonding, physical and chemical adsorptions to create core-shell morphology. It is expected that the physical and chemical bonds will stabilize the magnetite nanoparticles from oxidation with oxygen as represented in Scheme 1 [29].

3.1. Characterization of capped magnetite NPs

It was previously reported that the mixtures of magnetite and maghemite was obtained from reaction of KI and $FeCl_3$ in the presence of I_2 as confirmed from FTIR analysis [26,27]. The chemical structure of iron oxide capped with EDTA in the presence and absence of I_2 was confirmed from FTIR spectra as represented in Fig. 5a and b. It was found that the appearance of broad band at 570 cm^{-1} (Fe-O stretching) elucidates that the iron oxide is magnetite.

The absence of bands at 650 and 750 cm^{-1} confirms that magnetite was not formed and indicates that the capping with EDTA stabilized the magnetite against oxidation reaction [28]. Moreover, the disappearance of a large and intense band at 3450 cm^{-1} that confirms that the hydroxyl groups surrounded to magnetite nanoparticles have been modified by EDTA. The presence of EDTA was confirmed by the appearance of bands at 1630 and 1450 cm^{-1} which are attributed to COOH and CH_2 stretching and indicated the functionalization of magnetite nanoparticles with the carboxylic or amine group of EDTA. The formation of pure magnetite using EDTA as capping agent was confirmed from X-ray diffraction as illustrated in Fig. 6a and b. The data showing a diffraction patterns of magnetite nanoparticles at (110), (220), (311), (400), (422), (511), and (622) which are the characteristics of the Fe_3O_4 crystal with a cubic spinel structure. The morphology of magnetite coated with EDTA in the presence and absence of I_2 was confirmed by TEM analysis as represented in Fig. 7a and b. The capping of magnetite with EDTA in the presence of I_2 (Fig. 7a) provides connected spherical nanoparticles. The absence of I_2 produced clusters of magnetite as confirmed from Fig. 7b. The presence of EDTA and iodine increase the colloidal stability and distribution increased with respect to bare Fe_3O_4 nanoparticles.

The colloidal stability of magnetite nanoparticles in the absence and presence of EDTA and I_2 was estimated by measuring the zeta

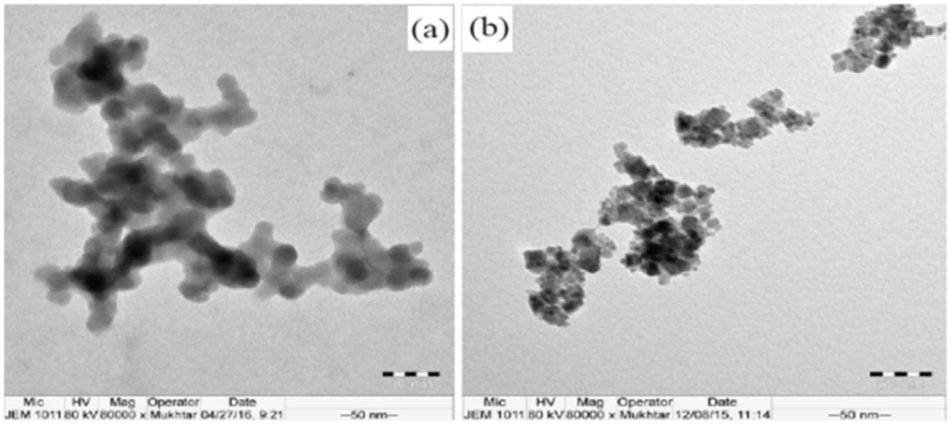

Fig. 7. TEM micrographs of the prepared magnetite (**a**) presence of EDTA/I_2 and (**b**) presence of EDTA without I_2.

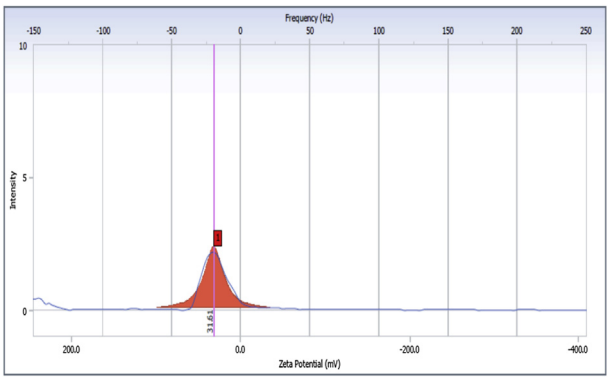

Fig. 8. Zeta potential of magnetite prepared in the presence of iodine.

potential as illustrated in Fig. 8. The data of zeta potential (mV) of magnetite with I_2, magnetite without I_2, magnetite capped with EDTA and I_2 and magnetite capped with EDTA without I_2 are 31.55, 14.8, 39.61 and −35.20 respectively. These data confirm that the dispersion stability of nanoparticle colloids increased when zeta potential increased more than positive or negative 25 mV. Accordingly, the presence of iodine and EDTA increased the dispersion stability of magnetite in aqueous solution. The negative value of zeta potential occurred when EDTA used as capping agent in absence of iodine. This means that the carboxylate groups of EDTA were not bonded with magnetite surfaces in absence of I_2. The particle size and polydispersity index (PDI) of uncapped and capped magnetite nanoparticles capped with EDTA in the presence and absence of I_2 were measured and illustrated in Fig. 9 (a–d). The data indicated that monodisperse nanoparticles have particle size of 104.3 nm was obtained for magnetite capped with EDTA in the presence of I_2. These data confirm that iodine binds so tightly to the particle surface to iron oxide particles that it impedes particle growth [30]. Fig. 10 shows the SEM images of pristine BiMnOx and it shows the fibrous needle shaped BiMnOx particles aggregated together to form the spherical shape morphology. Fig. 11a–b shows the BiMnOx (214) magnetite nanocomposite, which shows the similar morphology of pristine BiMnOx and after magnetite deposition results in reduce the particle size of BiMnOx. The elemental composition of the respective element present in the nanocomposite are shows in the inset of Fig. 11c. Major content of manganese, oxygen and carbon are observed in wt% compared to iron content. Bismuth content present in nanocomposite is confirmed by high resolution TEM-EDX. The more iron content deposition or incorporation into the matrix of BiMnOx is influence by the preparation method of magnetite nanoparticle. Fig. 12 shows the TEM images of magnetite (211)-BiMnOx nanocomposite, the tubular morphology of BiMnOx is acted as porous template to alter the magnetite nanoparticle into nanorod structures, which is very clearly seen in the TEM images of Fig. 12a. Fig. 12 a and b shows the nanotubes shapes of metal rich magnetite nanoparticle deposition on manganese oxide nanotubes and some of the magnetite particle inserted into the tubular structure of BiMnOx (Fig. 12 c and d). HR-TEM-EDX data of magnetite (211)-BiMnOx nanocomposite is shown in Fig. 12b, which is clearly indicate the presence of bismuth incorporation and iron content presence in the nanocomposite. The length of individual BiMnOx nanotube is observed around 30–50 nm.

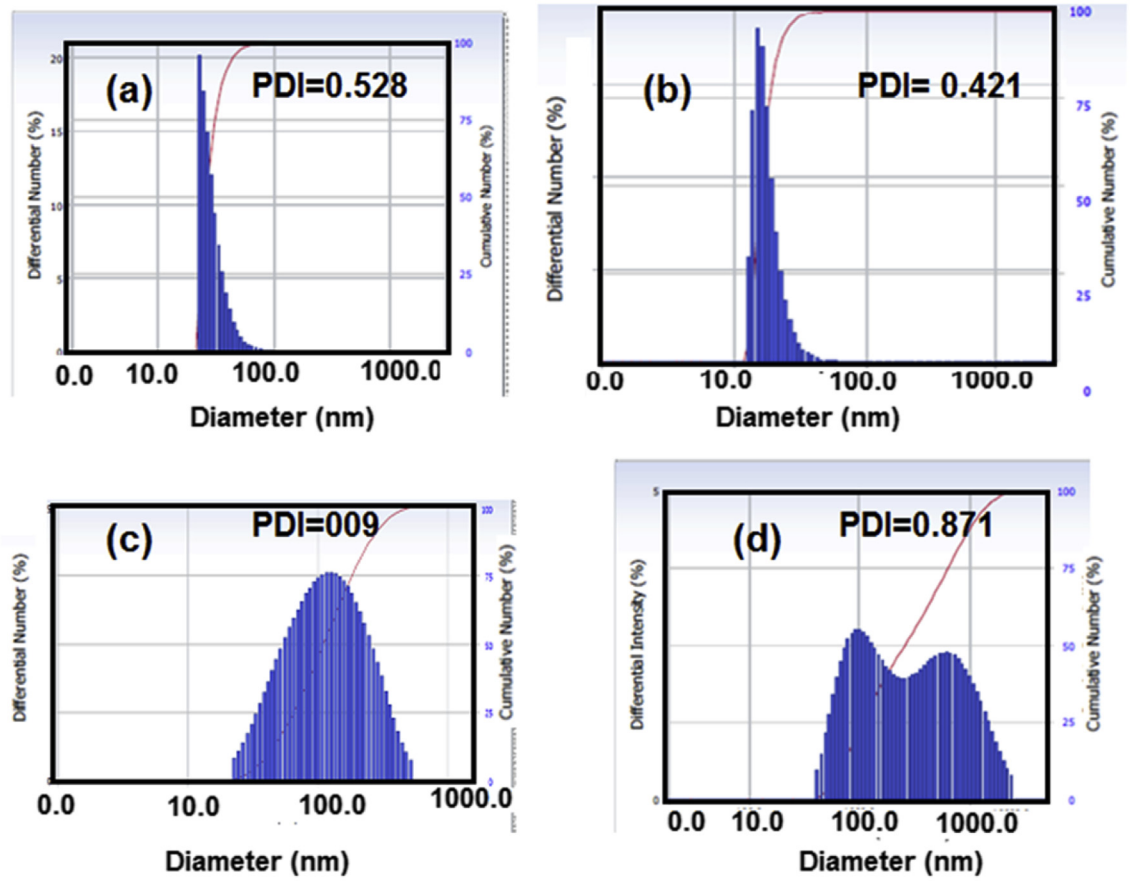

Fig. 9. DLS of the prepared magnetite (**a**) absence of iodine (211); (**b**) presence of iodine (212); (**c**) presence of EDTA/Iodine (213) and (**d**) presence of excess EDTA (214).

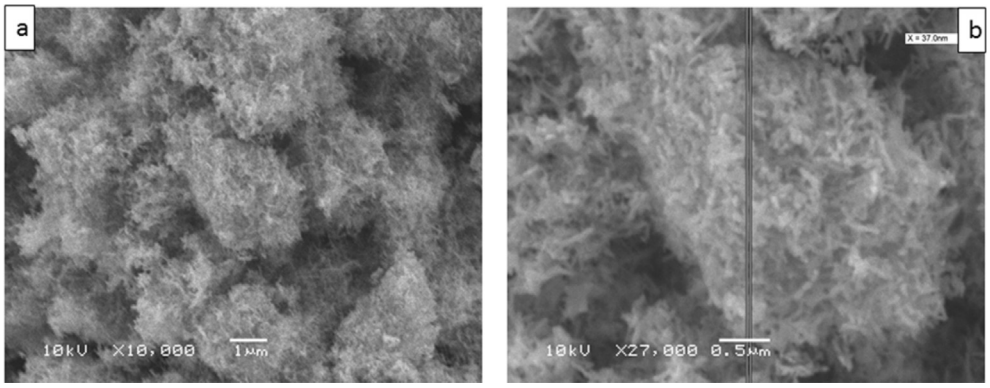

Fig. 10. SEM images of pristine BiMnOx nanotube.

The BET surface area and N_2 adsorption-desorption curves are shown in Fig. 13. The sorption-desorption isotherm shapes are observed similarly with Type IV and H2 type hysteresis, the hysteresis loop low relative pressures between 0.4 and 0.9, indicating the presence of ink-bottle pores with narrow necks and wider bodies, which are formed between primary crystallites. It contains both micro and meso pores structure with average pore volume value and the total Pore volume 2×10^{-2} cc/g at $P/P_0 = 0.36$. The catalytic sorption and removal capacity of phenol on magnetite deposited BiMnOx nanotubes is tested by batch method [31–33]. The removal capacity and adsorption capacity of each sample are shown in Fig. 14. Magnetite (211 and 212) nanoparticle deposited

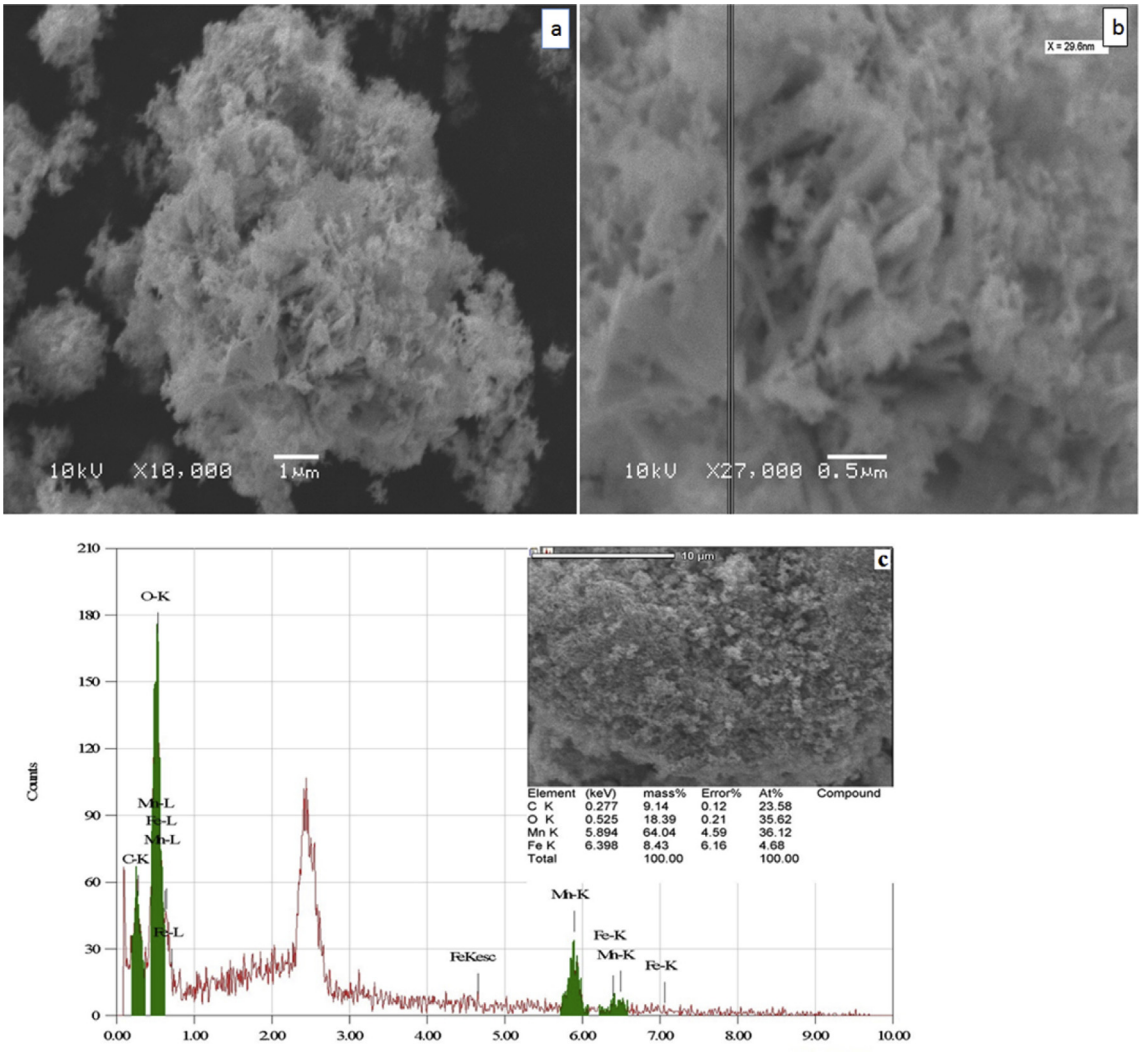

Fig. 11. SEM-EDX data of magnetite (214) deposited BiMnOx nanotube.

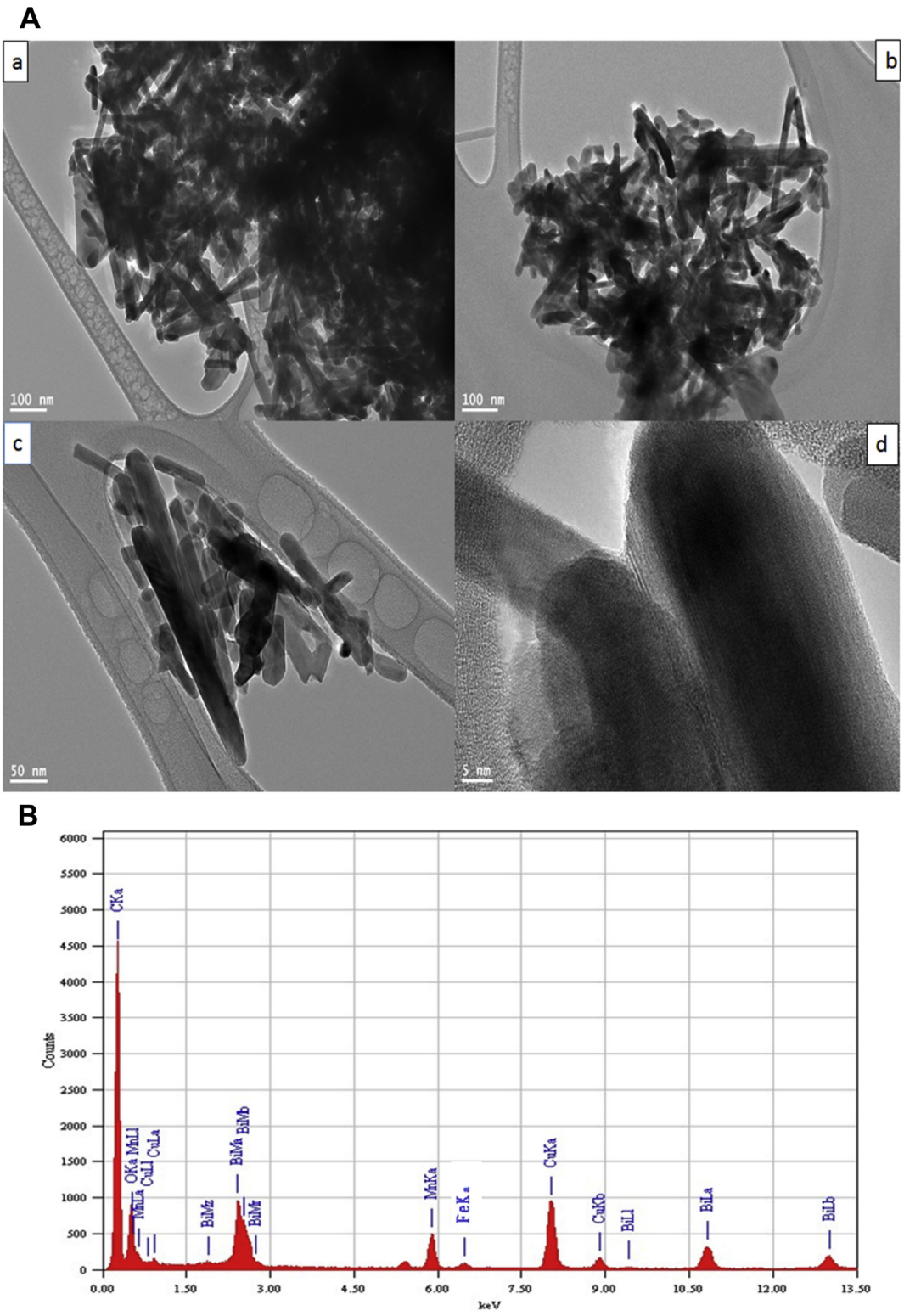

Fig. 12. a TEM images of magnetite (211) deposited BiMnOx nanotube. b TEM-EDX images of magnetite (211) deposited BiMnOx nanotube.

BiMnOx are showing higher removal capacity at short duration of time (within 1 h of reaction time). Magnetite (213) incorporated BiMnOx catalyst showing little lower adsorption capacity than other magnetite deposited BiMnOx catalysts due excess carbon deposit on the surface of manganese oxide surface [34]. In conclusion, magnetite nanoparticle prepared in the presence of iodine showing much higher catalytic activity compared iodine and EDTA stabilized catalyst. To use of excess EDTA results in decrease in catalytic activity of the magnetite nanoparticles deposited on BiMnOx support. Therefore, present study explained the optimization of synthesis reaction condition for magnetite formation to prepare the active magnetite nanoparticle and followed by

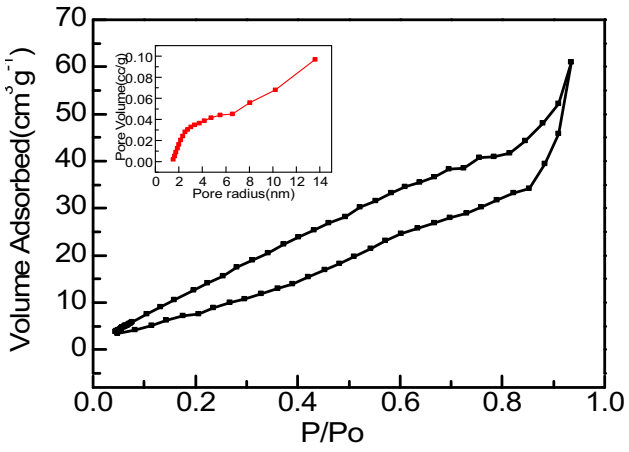

Fig. 13. N_2 sorption-desorption behavior and pore size diagram of pristine BiMnOx nanotube.

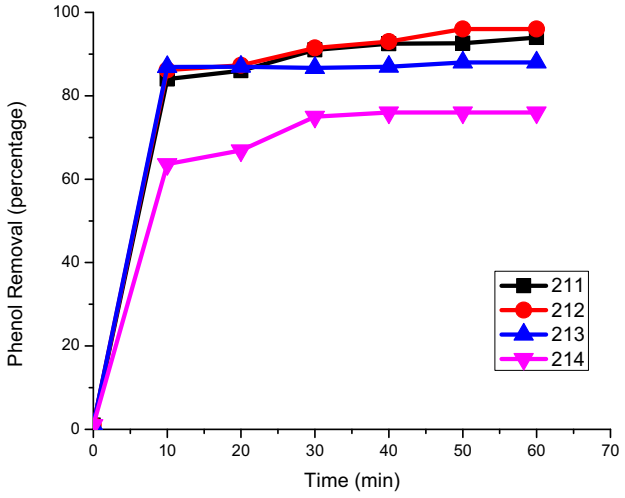

Fig. 14. Phenol sorption and removal capacity of as prepared magnetite deposited BiMnOx nanocomposite.

deposition in BiMnOx nanocomposite. The magnetite/BiMnOx nanocomposites could provide potential application in the field of visible light driven photo catalysis, drug delivery application and supercapcitor based device fabrication.

4. Conclusion

Magnetite nanoparticle and bismuth doped manganese oxide nanotube with fine particle size are synthesized successfully by different method by adopting various capping agent. Magnetite nanoparticle was further deposited on porous Bi-MnOx nanotube by ultra-sonication method. DRS-UV-Vis data showing that the fine tuning of band gap for magnetite deposited Bi-MnOx nano-composite materials. HR-TEM images are confirming the bismuth doping as well as nanotube structure formation for magnetite deposited Bi-MnOx. The as prepared materials showing good sorption capacity and removal capacity (upto 90%) for phenol removal at short time duration. In future the prepared nano-composite materials could act as the potential application in catalysis and electrochemical supercapcitor device fabrication.

Acknowledgement

This project was financially supported by King Saud University, Deanship of Scientific Research, Research Chairs.

References

[1] R. Jothiramalingam, B. Viswanathan, T.K. Varadarajan, Catal. Commun. 6 (2005) 41–45.
[2] R.A. Revia, M. Zhang, Mater. Today 9 (2016) 157–168.
[3] R. Jothiramalingam, M.K. Wang, J. Hazard. Mater. 147 (2007) 562–569.
[4] M. Abecassis-Wolfovich, R. Jothiramalingam, M.V. Landau, M. Herskowitz, B. Viswanathan, T.K. Varadarajan, Appl. Catal. B Environ. 59 (2005) 91–98.
[5] S. Khilari, S. Pandit, M.M. Ghangrekar, D. Das, D. Pradhan, RSC Adv. 3 (2013) 7902–7911.
[6] R. Jothiramalingam, M.K. Wang, J. Porous Mater. 17 (2010) 677–683.
[7] Y. Wang, A. Yuan, X. Wang, J. Solid State Electrochem 12 (2008) 1101–1107.
[8] S. Liang, F. Teng, G. Bulgan, R. Zong, Y. Zhu, J. Phys. Chem. C 112 (2008) 5307–5315.
[9] J. Zhang, X.S. Zhao, Carbon 52 (2013) 1–9.
[10] Y. Lv, H. Li, Y. Xie, S. Li, J. Li, Y. Xing, Y. Song, Particuology 15 (2014) 34–38.
[11] O. Iglesias, M.A. Fernandez de Dios, M. Pazos, M.A. Sanroman, Environ. Sci. Pollut. Res. Int. 20 (2013) 5983–5993.
[12] H. Li, H. Lei, K. Chen, C. Yao, X. Zhang, Q. Leng, W. Wang, J. Chem. Technol. Biotechnol. 86 (2011) 398–405.
[13] X.Y. Li, Y. Huang, C. Li, J.M. Shen, Y. Deng, Chem. Eng. J. 260 (2015) 28–36.
[14] Y. Wang, H. Zhao, S. Chai, Y. Wang, G. Zhao, D. Li, Chem. Eng. J. 223 (2013) 524–535.
[15] L.J. Xu, J.L. Wang, Environ. Sci. Technol. 46 (2012) 10145–10153.
[16] Z.Q. He, C. Gao, M.Q. Qian, Y.Q. Shi, J.M. Chen, S. Song, Ind. Eng. Chem. Res. 53 (2014) 3435–3447.
[17] S. Navalon, A. Dhakshinamoorthy, M. Alvaro, H. Garcia, ChemSusChem 4 (2011) 1712–1730.
[18] M.X. Yang, J. Ma, Y.R. Sun, X.Z. Xiong, C.L. Li, Q. Li, J.H. Chen, Chem. J. Chin. Univ. Chin. 35 (2014) 570–575.
[19] S. Navalon, M. Alvaro, H. Garcia, Appl. Catal. B Environ. 99 (2010) 1–26.
[20] Mingyu Wei, Yang Ruan, Shilu Luo, Xiaoxia Li, Aihua Xu, Ping Zhang, New J. Chem. 39 (2015) 6395–6403.
[21] S.L. Viñas, K. Simeonidis, Z.-A. Li, Z. Ma, E. Myrovali, A. Makridis, D. Sakellari, M. Angelakeris, U. Wiedwald, M. Spasova, M. Farle, J. Magn. Magn. Mater. 415 (2016) 20–23.
[22] J. Zhu, S. Tang, H. Xie, Y. Dai, X. Meng, ACS Appl. Mater. Interfaces 6 (20) (2014) 17637–17646.
[23] Gamal A. El-Mahdy, Ayman M. Atta, Hamad A. Al-Lohedan, J. Taiwan Inst. Chem. Eng. 45 (2014) 1947–1953.
[24] Ayman M. Atta, Z.F. Aki, Mater. Chem. Phys. 163 (2015) 253–261.
[25] M. Augustin, D. Fenske, I. Bardenhagen1, A. Westphal, M. Knipper, T. Plaggenborg, J. Kolny-Olesiak, J. Parisi, Beilstein J. Nanotechnol. 6 (2015) 47–59.
[26] Ayman M. Atta, Hamad A. Al-Lohedan, Sami A. Al-Hussain, Molecules 19 (8) (2014) 11263–11278.
[27] A.M. Atta, A.K.F. Dyab, Coated Magnetite Nanoparticles, Method for the Preparation Thereof and Their Use, March 2013. EP 2804186 A1, 18.
[28] M.I. Khalil, Process for Preparing Magnetic (Fe_3O_4) and Derivatives Thereof, January 2013. EP 2505558 A1, 16.
[29] T. Madrakian, A. Afkhami, M.A. Zolfigo, M. Ahmadi, N. Koukabi, Nano-Micro. Lett. 4 (2012) 57–63.
[30] T.K. Nguyen, A. Thanha, A.W. Luke, Nano Today 5 (2010) 213–230.
[31] G.V. Sokol'skiia, S.V. Ivanovaa, N.D. Ivanovab, E.I. Boldyrevb, T.F. Lobunetsc, T.V. Tomilac, J. Water Chem. Technol. 34 (2013) 227–233.
[32] J. Liu, W. Wang, Y. Xie, Y. Huang, Y. Liu, X. Liu, R. Zhao, G. Liu, Y. Chen, J. Mater. Chem. 2011 (2011) 9232–9238.
[33] S. Banerjee, D.H. Chen, J. Hazard. Mater. 147 (2007) 792–799.
[34] N. Wang, L. Zhou, J. Guo, Q. Ye, J. Lin, J. Yuan, Appl. Surf. Sci. 316 (2014) 267–273.